11
Predicting Polaronic Defect States by Means of Generalized Koopmans Density Functional Calculations

Stephan Lany

11.1
Introduction

In semiconductors and insulators, non-isovalent atomic substitution critically controls the electrical behavior by introduces carriers (electrons or holes), and the utilization of such "doping" [1] lies at the heart of modern semiconductor technology. The dopants are generally classified into two categories, "shallow" and "deep" [2]: Shallow donor or acceptor states, respectively, can be thermally excited into the conduction band minimum (CBM) or the valence band maximum (VBM) thereby releasing the carriers that give rise to *n*- or *p*-type conductivity. Deep states, in contrast, are often undesired, since they can cause carrier trapping and recombination. In order to theoretically model a doped semiconductor it is, therefore, indispensable to be able to predict whether an impurity or defect acts as a shallow or as a deep center and to predict accurately the energy levels relative to the respective band edges (CBM or VBM). (In the following, we will use the term "semiconductor" in the wider sense as comprising also wide-gap materials and insulators). In this paper, we review recent work on a particular class of deep defects, *i.e.*, the impurity- or defect-bound small polarons [3], which are atomically localized and strongly bound defect states that create large lattice distortions.

The modeling of isolated point defects in semiconductors requires to treat in the order of 100 atoms, *e.g.*, in a supercell method, which necessitates rather efficient electronic structure methods. Thus, most total-energy calculations for defects in semiconductors have so far been performed using density functional theory (DFT) [4, 5] in its standard local density approximation (LDA) [6–8] for exchange and correlation, or gradient corrected versions thereof (GGA) [9–11]. However, in many cases, these density functional approximations (DFA) fail even qualitatively in the prediction of defect states with localized wavefunctions. For example, experiment has shown that acceptor-bound holes in many oxides are deep centers having wavefunctions that are centered at single oxygen atoms, *e.g.*, $\underline{Si}O_2$:Al [12], $\underline{Zn}$O:Li [13], or the singly charged Zn vacancy (V_{Zn}^{-}) in ZnO [14, 15] and ZnSe [16]. In contrast, DFA predicts in all these cases that the hole-wavefunction is distributed over the equivalent

Advanced Calculations for Defects in Materials: Electronic Structure Methods, First Edition.
Edited by Audrius Alkauskas, Peter Deák, Jörg Neugebauer, Alfredo Pasquarello, and Chris G. Van de Walle.

O atoms neighboring the defect [17–21]. All these cases are characterized by an open-shell electronic configuration of the bound state, *e.g.*, the $a_1^2\, t_2^5$ configuration of Li_{Zn} in ZnO (using the notation of the approximate T_d point group symmetry of Li_{Zn}). The wrong wave-function localization can be understood as resulting from the residual self-interaction error of DFA, leading to an insufficient energy splitting between occupied and unoccupied states [18, 19]. The wave-function localization and resulting structural properties can be corrected by a range of theoretical methods, such as Hartree–Fock (HF) [17, 22], hybrid functionals [21, 23–25], screened exchange [26], DFA + U applied to O-p orbitals [27–30], self-interaction correction [31, 32], or our recently introduced hole-state potential [19, 20] which, although related to DFA + U, is constructed such to avoid the rather uncontrolled modification of the defect-free host-bandstructure when DFA + U is applied to the anion p-states [19].

For illustration, we compare in Figure 11.1 the calculated spin–density of the Li_{Zn}^0 center in ZnO in DFA and after applying the correction of Ref. [19]. (Note that the spin–density isosurface shown in Figure 11.1 closely resembles the wave-function-square of the unoccupied acceptor state. We prefer to show the spin–density, because this quantity is probed in magnetic resonance experiments [13].) We see that in DFA the acceptor state is not only delocalized over the neighboring oxygen atoms, but spreads over the entire supercell. This behavior is clearly that of a shallow state, similar to what one would expect from effective-mass theory [33, 34]. Accordingly, the acceptor ionization energy is relatively small in DFA, around 0.1–0.2 eV [35, 36]. However, both the delocalization over many atomic sites (Figure 11.1a) and the shallow acceptor level are inconsistent with experiment, which shows localization on a single O atom [13] and an much deeper acceptor state around 0.8 eV [37, 38]. Applying the hole-state potential of Ref. [19], the acceptor state becomes localized on a single O atom leading to a local magnetic moment at this O site, and strong structural relaxations occur which break the (approximate) tetrahedral (T_d) local symmetry around the Li impurity (see Figure 11.1). Alternatively, the mixing of Fock exchange into the DFA Hamiltonian, as done in hybrid-functionals [39–41] has very

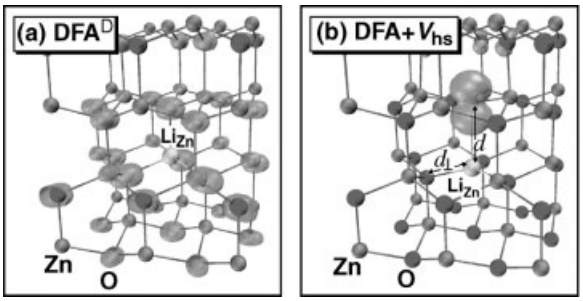

Figure 11.1 (online colour at: www.pss-b.com) Spin–density isosurface (green) of the Li_{Zn} acceptor in ZnO. In standard DFA (a), the acceptor wavefunction is effective-mass like and the structure is symmetric ($d_{Li-O} = 2.02$ Å). (b) After correction by the onsite potential V_{hs} the acceptor state is localized on a single O atom, and the structure is symmetry broken ($d_\perp = 1.91$ Å; $d_{||} = 2.71$ Å) (Ref. [19]).

similar effects on the defect geometry and the localization of the acceptor state [21, 24] of Li_{Zn}.

By phasing in the on-site correction for O-*p* orbitals, we found in Ref. [19] that the geometry, the wavefunction localization, and the local magnetic moment exhibit an almost "digital" behavior, *i.e.*, the change from the situation of Figure 11.1a to that of Figure 11.1b occurs abruptly above a critical value of the on-site potential and then changes very little when further increasing the potential strength parameter. Similarly, hybrid-functional calculations of the Al_{Si} center in SiO_2 using the B3LYP functional [39] with 20% Fock exchange did not restore the localization of the hole on a single oxygen site [17, 18], but the localization kicks in when the fraction of Fock exchange is increased [23]. Therefore, a guiding principle is desired that helps to determine appropriate parameters for such methods. Whereas the correct description of the structural and magnetic properties mostly require that the parameterized DFA correction (U, V_{hs}, Fock-exchange, *etc.*) is sufficient to stabilize the localized solution above the critical threshold, an accurate determination of these parameters is even more important when one is interested in energy differences between the localized and delocalized states to determine, for instance, acceptor binding energies in oxides, because these change continuously with the strength of the parameterized correction, *e.g.*, the on-site potential V_{hs} [19]. Indeed, different parameterizations of hybrid-functionals have also led to rather different ionization energies for Li in ZnO [21, 24]. We now formulate a generalized Koopmans condition [19] that can serve as such a guiding principle to determine appropriate parameters for DFA corrections.

11.2
The Generalized Koopmans Condition

The Hohenberg–Kohn theorem [4] of DFT can be extended to fractional electron numbers N, describing a separated open system with fluctuating electrons [42, 43]. The *exact* total energy is then a piecewise linear function $E(N)$ with a discontinuous slope at integer N. In DFA, however, $E(N)$ is generally a convex function [43, 44], due to the approximate nature of the local density formalism. In order to relate the curvature of $E(N)$ to the behavior of Kohn–Sham (KS) single particle energy e_i when changing the occupation $0 \leq n_i < 1$ of the state i, we employ Janak's theorem [45, 46],

$$\mathrm{d}E(n_i)/\mathrm{d}n_i = e_i, \tag{11.1}$$

and find that the convexity of $E(N)$ is caused by a shift of e_i to higher energies during the occupation of state i in DFA, *i.e.*,

$$\begin{aligned} &\mathrm{d}^2 E\,(n_i)/\mathrm{d}n_i^2 > 0, \quad \text{or} \\ &\mathrm{d}e_i(n_i)/\mathrm{d}n_i > 0, \end{aligned} \tag{11.2}$$

(Note that we assume that the density functional does not have an explicit discontinuity [47, 48], which is the case for all methods considered here).

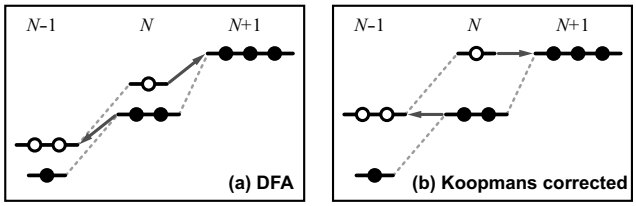

Figure 11.2 (online colour at: www.pss-b.com) Schematic illustration of the single particle energy shifts upon electron addition or removal in DFA (a) and after enforcing the generalized Koopmans condition (b). In (b), the state whose occupancy is changed (red arrows) maintains a constant energy.

For illustration, Figure 11.2 shows the single particle energy scheme for electron removal from or electron addition into a partially occupied state. This situation occurs, *e.g.*, in case of the p^5 configuration of the isolated F atom [43, 49], where the three F-*p* (say, p_x, p_y, and p_z) orbitals of the spin-down channel are occupied by only two electrons. As illustrated in Figure 11.2a, the energy gap between the occupied and the unoccupied orbitals is usually rather small (or even vanishes) in DFA. For example, we obtained a gap of only 0.7 eV for the F-atom in its non-spherical, symmetry-broken DFA ground state [49]. When an electron is added, the energy of all three states increases, and the gap closes due to energetic degeneracy when all states are occupied (Figure 11.2a). Conversely, when an electron is removed, the energy of all states is lowered. Whereas the change of the single particle energy of *one state* due to the electron addition into *another state* reflects simply the increased Coulomb repulsion, the energy change of the highest state i following the change of its *own* occupation reflects a spurious self-interaction effect of DFA, which gives rise to erroneous convexity of $E(N)$, *cf.* Eq. (11.2). Indeed, the correct situation that leads to the linearity of $E(N)$,

$$\begin{aligned} &\mathrm{d}^2E(n_i)/\mathrm{d}n_i^2 = 0, \quad \text{or} \\ &\mathrm{d}e_i(n_i)/\mathrm{d}n_i = 0, \end{aligned} \tag{11.3}$$

requires that the energy of the state i (*i.e.*, the one whose occupation changes) remains constant during electron addition or removal, as shown in Figure 11.2b. If the DFA is corrected such to fulfill this requirement, we obtain for the electron addition energy (negative of the electron affinity A)

$$E(N+1) - E(N) = e_i(N), \tag{11.4}$$

by integration of Janak's theorem, or, equivalently,

$$E(N-1) - E(N) = -e_i(N), \tag{11.5}$$

for the electron removal energy (ionization potential I). In this case, the KS eigenvalue e_i of the state i acquires the meaning of a quasi-particle energy. Since, the index i refers to the state whose occupancy changes, $e_i(N)$ is either the lowest unoccupied state of the N electron system in case of electron addition [Eq. (11.4)], or it

is the highest occupied state system of the N electron system in case of electron removal [Eq. (11.5)] (see Figure 11.2). Thus, if the conditions (4) and (5) are met, the single-particle gap equals the quasi-particle gap $I - A$, which, *e.g.*, in case of the above mentioned example of the F-atom is 14 eV, much larger than the 0.7 eV single-particle energy gap in DFA [49] (*cf.* Figures 11.2a and b).

Equation (11.4) [and the equivalent Eq. (11.5)] resembles the Koopmans theorem which states an *approximate equality* in HF theory [50]. We emphasize, however, that here it has instead the meaning of a *condition* that has to be made fulfilled for parameterized corrections of DFA, such as the on-site potentials defined in Ref. [19], or the appropriate fraction of Fock-exchange in hybrid-functionals (see below). To clarify the relation between Eq. (11.4) and the Koopmans theorem, we consider that the electron addition energy – for a fixed structural geometry – can be expressed as [45, 51]

$$E(N+1)-E(N) = e_i(N) + \Pi_i + \Sigma_i. \tag{11.6}$$

Here, Π_i is the SI energy after electron addition to the orbital i under the constraint of the wave-functions being fixed at the initial-state, and Σ_i is the energy contribution arising due to wave-function relaxation. The original Koopmans theorem [50] was formulated for HF theory, where $\Pi_i \equiv 0$ holds rigorously, as an *approximation* which is good only when relaxation effects are small. In solids, however, the (negative) relaxation energy $\Sigma_i < 0$ is usually not negligible, in particular because dielectric screening leads to a significant charge rearrangement (requiring wave-function relaxation) following the electron addition into the state e_i. Indeed, by comparing Eqs. (11.4) and (11.6) we see that due to $\Sigma_i < 0$, the HF eigenenergy $e_i(N)$ of the initially unoccupied state is higher than the electron addition energy, just opposite to the situation in DFA. Accordingly, HF calculations exhibit the well-known [43, 44] concave behavior $\mathrm{d}^2E(n_i)/(n_i)\mathrm{d}n_i^2 < 0$, opposite to the convex behavior of DFA. The correct linearity of $E(N)$ [Eq. (11.3)] is obtained in between the DFA and HF limits, when the SI energy Π_i and the relaxation energy Σ_i cancel each other, *i.e.*, $\Pi_i + \Sigma_i = 0$.

11.3
Adjusting the Koopmans Condition using Parameterized On-Site Functionals

By avoiding the necessity to evaluate linearity of the function $E(N)$ explicitly, the generalized Koopmans condition, Eqs. (11.4) and (11.5) serve as a convenient tool to restore the correct behavior of the functional upon variation of the occupation. In order to compensate for the convex shape of $E(N)$ in DFA, one needs a suitable, parameterized perturbation of the DFA Hamiltonian that allows to make Eqs. (11.4) or (11.5) satisfied by adjustment of the parameter. Based on the observation that DFA and HF theory show opposite curvatures of $E(N)$, one obvious possibility is mix DFA and the Fock exchange in hybrid-functionals, so to balance the two opposite behaviors. A computationally less expensive method is DFA + U [52], which has indeed been successful in restoring the correct localization of the Al_{Si} defect in

SiO_2 [27]. However, the application of DFA + U to anion-p states, as needed for the treatment of, *e.g.*, O-localized holes (*cf.* Figure 11.1b), is somewhat problematic: the DFA + U potential, *e.g.*, in its simplified form of Ref. [53],

$$V_{\mathrm{U}} = (U-J)\left(\frac{1}{2}-n_{m,\sigma}\right), \tag{11.7}$$

depends on the atomic orbital projected occupancy $n_{m,\sigma}$ for the m-sublevels of spin σ. On the other hand, the anion-p states are generally much less localized than d-states on which DFA + U is typically applied, and the respective occupancy, *e.g.*, of an O-site in defect free environment of a pure oxide host is therefore considerably smaller than the nominal full occupancy $n_{m,\sigma}=1$ expected for O(−II) anions, and it depends on the integration radius used for DFA + U. For example, we found [19] for the O-p occupancy in pure, defect-free ZnO, $n_{m,\sigma}=0.4$–0.7 depending on the size of the integration radius associated with different pseudopotentials. Considering the form of the DFA + U potential, Eq. (11.7), we see that DFA + U for O-p has a rather uncontrolled effect on the O-p host states, creating either an attractive (if $n_{m,\sigma}>0.5$) or a repulsive (if $n_{m,\sigma}<0.5$) potential causing a significant and uncontrolled distortion of the band structure of the pure oxide, even in the absence of any defect or impurity. For example, application of DFT + U to the defect-free oxide would decrease or increase the band gap (by shifting the O-p states down or up) depending on the choice of the pseudopotential.

In order to avoid the uncontrolled side effects of DFA + U, we defined in Ref. [49, 54] a "hole-state potential" of the form

$$V_{\mathrm{hs}} = \lambda_{\mathrm{hs}}(1-n_{m,\sigma}/n_{\mathrm{host}}), \tag{11.8}$$

which can be created by superposition of the occupation dependent DFA + U potential, Eq. (11.7), and the occupation-independent non-local external potential of Ref. [55]. Here, the reference occupation n_{host} is taken as the occupancy in the defect-free oxide host, so that the V_{hs} vanishes for all normally occupied O-p orbitals in the pure host. The parameter λ_{hs} controls the strength of the hole-state potential and will be adjusted so to match the Koopmans condition. If now a hole polaron is trapped at an O-site, this will cause a much lower occupancy $n_{m,\sigma}$ for the sublevel hosting the hole (*e.g.*, the O-p_z orbital shown in Figure 11.1b), creating a repulsive potential for this level, and therefore stabilizing the localized hole. The effect of V_{hs} is illustrated schematically in Figure 11.3, showing for the Li acceptor in ZnO the O-p orbital energies (minority-spin, $\sigma=\downarrow$) for the O neighbor that has the hole trapped. Since these O-p orbitals occur as resonant states centered at energies below the VBM, the small splitting between the occupied and unoccupied sub-levels in DFA (*cf.* Figure 11.2) is not enough to lift the unoccupied level into the gap. Consequently, the hole relaxes to the VBM, and occupies the shallow effective-mass like level, as shown in Figure 11.1a. The increased splitting between the occupied and unoccupied sublevels due to the hole-state potential V_{hs} moves the localized hole state into the gap, thereby creating an acceptor state that is localized on a single O-atom (Figure 11.1b).

From the level diagram shown in Figure 11.3, one can expect that a minimum strength of V_{hs} [controlled via the strength parameter λ_{hs}, see Eq. (11.8)] is needed to

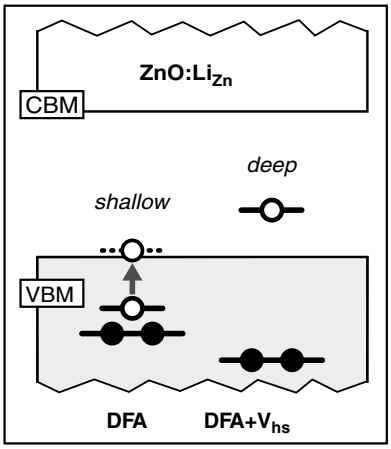

Figure 11.3 (online colour at: www.pss-b.com) Schematic illustration of the occupied and unoccupied single particle energies for the oxygen hole due to Li_{Zn} in ZnO. In DFA (left), the localized hole at the O-site is unstable and relaxes into the shallow effective-mass state just above the VBM. Applying the hole-state potential V_{hs} (right) increases the splitting which stabilizes the localization of the hole in one O-*p* sub-orbital (*cf.* Figure 11.1).

lift the unoccupied O-*p* state into the gap and to stabilize the polaronic hole state. Indeed, when we phase-in V_{hs}, we observe that beyond a critical value $\lambda_{hs} > \lambda_{hs}^{cr}$ of the hole state potential, the symmetry breaking occurs and a strong local magnetic moment develops at the O-site at which the hole is localized, as shown in Figure 11.4a. In this calculation, in which we used the exchange-correlation functional of Ref. [11] for the underlying DFA, the condition Eq. (11.4) is fulfilled for $\lambda_{hs}^{lin} = 4.3$ eV [19] (see Figure 11.4b), at which point the correct linear behavior [*cf.* Eq. (11.3)] is recovered. Since, λ_{hs}^{lin} lies well above the critical value λ_{hs}^{cr} required to stabilize the polaronic state (see Figure 11.4b), the polaron state is predicted to be the physically correct state. Note that when Eqs. (11.4) or (11.5) are employed to determine the appropriate value for the parameterized functional (*e.g.*, λ_{hs} for the on-site potential V_{hs}), one has to correct for supercell finite-size effects that affect both total energies $E(N)$ (see Refs. [49, 54]) and single-particle energies $e(N)$ [56] in case the electron number N corresponds to a charged defect state.

11.4
Koopmans Behavior in Hybrid-functionals: The Nitrogen Acceptor in ZnO

While HF theory was successful in describing qualitatively correctly the localization of holes on single oxygen sites, *e.g.*, for the Al_{Si} defect in SiO_2 (smoky quartz) [17, 18], or Li_{Mg} in MgO [22], it does not provide a quantitative description: *e.g.*, it predicts much too large band gaps and exceedingly large hole binding energies, *e.g.*, the hole state bound at an O-neighbor of Li_{Mg} in MgO was found roughly 10 eV above the valence band in Ref. [22]. Accordingly HF predicts often polaronic carrier trapping

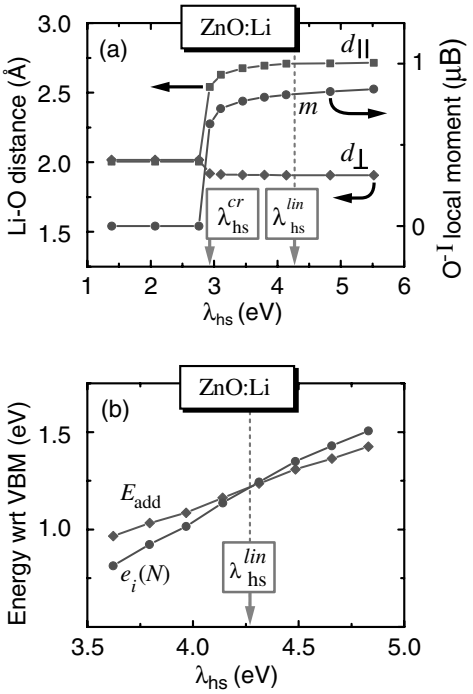

Figure 11.4 (online colour at: www.pss-b.com) (from Ref. [19]). (a) Structural and magnetic properties of the Li_{Zn} impurity in ZnO, as a function of the hole-state potential strength λ_{hs}. The polaronic state is stable above a critical value $\lambda_{hs} > \lambda_{hs}^{cr}$. The distance $d_{||}$ between Li and the O atom with the trapped hole becomes larger than the distance $d_{\perp}$ between Li and the O atoms in the basal plane. (*cf.* Figure 11.1b), and a strong local magnetic moment m occurs. (b) The electron addition energy $E_{add} = E(N+1) - E(N)$ and the energy eigenvalue $e_i(N)$ of the initially unoccupied acceptor state of Li. λ_{hs}^{lin} marks the value of λ_{hs} for which Eq. (11.4) is satisfied.

even in cases where it should not [57]. However, a reasonable compromise may be achieved by mixing only a fraction of the non-local Fock exchange into the DFA Hamiltonian. The non-local exchange potential in such hybrid-functionals has the general form

$$V_x^{nl}(\boldsymbol{r},\boldsymbol{r}') = -\alpha \sum_i \frac{\psi_i^*(\boldsymbol{r}')\psi_i(\boldsymbol{r})}{|\boldsymbol{r}-\boldsymbol{r}'|} f(|\boldsymbol{r}-\boldsymbol{r}'|), \tag{11.9}$$

where the parameter α and the attenuation function f vary among different formulations of hybrid-functionals, *e.g.*, B3LYP [39] ($\alpha = 0.2, f = 1$), PBEh [40] ($\alpha = 0.25, f = 1$), HSE [41] [$\alpha = 0.25$, $f = \mathrm{erfc}(\mu|\boldsymbol{r}-\boldsymbol{r}'|)$], or screened exchange [58–60] [$\alpha = 1$, $f = \exp(-k_{TF}|\boldsymbol{r}-\boldsymbol{r}'|)$]. For suitable parameters, such hybrid-functional calculations give reasonable band gaps, and therefore are increasingly applied for the prediction of defects in semiconductors [61–64]. (Note that the mentioned functionals further differ in the amount of semi-local gradient corrections for exchange and correlation,

which has, however, only minor effects on the band-structure properties). Hybrid-functionals have also been used to describe anion-localized hole states for defects in various oxides, *i.e.*, those cases where standard DFA fails even qualitatively, like Al_{Si} in SiO_2 [23], Al_{Ti} in TiO_2 [65], and Li_{Zn} in ZnO [21, 24].

Since, as discussed above, HF theory exhibits the opposite $E(N)$ non-linearity (concave) of DFA (convex), the mixture of DFA and Fock exchange can in principle also be used to cancel the non-linearity of $E(N)$, *i.e.*, to make the generalized Koopmans condition, Eq. (11.4), fulfilled. Typically, however, hybrid-functional parameters are either taken from the pre-defined standards of the respective hybrid-functional formulation [21, 66] or are adjusted to match the experimental band gap [24, 64], and neither choice guarantees that the cancellation of non-linearity is complete. Indeed, some previous hybrid-functional calculations showed deviation from experimentally established facts, either quantitatively (ZnO:Li, Ref. [21]) or even qualitatively (SiO_2:Al, Refs. [17, 18]). The ability of hybrid-functionals to match the generalized Koopmans condition was recently addressed for defects in elemental semiconductors [67], and for the case of the N_O acceptor in ZnO [68].

Acceptor-doping of ZnO with nitrogen is subject of a controversy in the experimental literature [69]. While substitutional N_O dopants are often considered as being shallow acceptors, magnetic resonance experiments found a strongly localized hole-wavefunction [70, 71] that is inconsistent with the picture of a shallow effective-mass acceptor.

As shown in Figure 11.5a, the N_O acceptor state is already at the DFA level more localized than an effective-mass state, in contrast to Li_{Zn} (Figure 11.1). In DFA, the hole-state has p_{xy} character (p-orbitals perpendicular to the crystal c-axis), stemming from a half-occupied e_g symmetric state. As seen in Table 11.1, the all four N−Zn nearest neighbor distances are almost identical. When applying the on-site potential V_{hs} to N-p orbitals (in addition to V_{hs} for the O-p orbitals as above), using a parameter λ_{hs} such to satisfy the Koopmans condition, Eq. (11.4), [72] the hole becomes largely localized within a single N-p_z orbital, stemming from an unoccupied a_1 symmetric state. The nearest neighbor distances are now strongly anisotropic, the Zn atom along the c-axis having an ∼0.2 Å larger distance from N than the Zn atoms in the basal plane (Table 11.1). Thus, in Koopmans-corrected DFT the partial occupancy is lifted, which leads to a Jahn–Teller relaxation, in accord with experimental interpretations [70, 71]. Comparing the effect of non-local Fock exchange with that of the on-site potential V_{hs}, we see that both methods predict very similar acceptor wave-functions (Figure 11.5) and defect geometries (Table 11.1).

Whereas the structural properties and the wavefunction localization of ZnO:Li showed an almost digital switching between the symmetric delocalized and the symmetry-broken localized configurations with variation of the potential strength parameter λ_{hs} (Figure 11.4a) the vertical acceptor ionization energy showed a more continuous variation with λ_{hs} (Figure 11.4b). A similar sensitivity on the details of the parameterized functional can be expected for the thermal (relaxed) acceptor ionization energy. Therefore, we examined the relation between the Koopmans behavior and the depth of the N_O acceptor level [68]: standard DFA calculations predicted the acceptor level 0.4 eV above the VBM [36]. When we apply DFA + U to account for

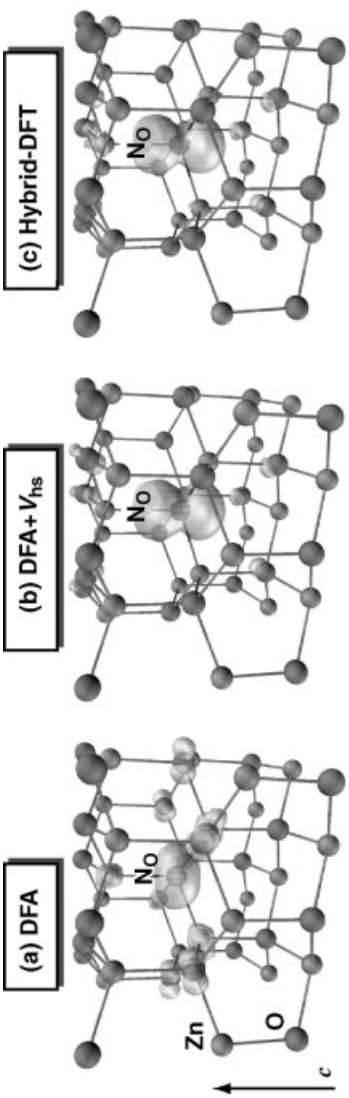

Figure 11.5 (online colour at: www.pss-b.com) (modified from Ref. [68]). Calculated spin–density (green: isosurface of 0.03 $\mu_B/\text{Å}^3$) of the neutral N_O^0 acceptor state in (a) standard DFA, (b) in Koopmans-corrected DFA with the onsite potential V_{hs}, and (c) in the HSE hybrid-functional. The arrow indicates the *c*-axis of the Wurtzite crystal.

Table 11.1 Properties of the neutral N_O acceptor in ZnO in different methods: the nearest neighbor N–Zn distances $d_{||}$ and $d_{\perp}$ (cf. Figure 11.1), the acceptor level $\varepsilon(0/1-)$, and the non-Koopmans energy Δ_{nK}.

	$d_{\|\|}/d_{\perp}$ (Å)	$\varepsilon(0/1-)$ (eV)	Δ_{nK} (eV)
DFA[a)]	1.93/1.95	$E_V + 0.74$	$+0.62$
DFA[a)] + V_{hs}	2.18/1.94	$E_V + 1.62$	0
HSE ($\alpha = 0.25$)	2.16/1.96	$E_V + 1.40$	-0.05
HSE ($\alpha = 0.38$)	2.16/1.96	$E_V + 2.05$	-0.40

a) see Ref. [73].

the too high Zn-*d* orbital energy and the resulting exaggerated *p*–*d* repulsion [49], we get already a quite deep acceptor level at 0.7 eV above the VBM (see Table 11.1). This, however does not yet address the Koopmans behavior of the N–*p* like hole state. Indeed, when we calculate the non-Koopmans energy $\Delta_{nK} = E(N+1) - E(N) - e_i(N)$ [*cf.* Eq. (11.4)], we find a large positive value $\Delta_{nK} = +0.6$ eV (Table 11.1) [72] originating from the convex $E(N)$ behavior of DFA. When the generalized Koopmans condition $\Delta_{nK} = 0$ is restored by means of the on-site potential V_{hs}, the acceptor level lies even much deeper at 1.6 eV above the VBM.

We further tested the Koopmans behavior of N_O in the HSE hybrid functional, comparing two different values for the parameter α [see Eq. (11.9)], *i.e.*, the "standard" value $\alpha = 0.25$ [40, 41], and an increased fraction of Fock exchange $\alpha = 0.38$, chosen such to reproduce the experimental band gap of ZnO [63]. We find that for $\alpha = 0.25$ the Koopmans condition is quite well fulfilled, although the band gap is still underestimated by about 1 eV. The acceptor level at 1.4 eV is close to the prediction with the on-site potential V_{hs}. A similar acceptor level was also found in a recent hybrid-functional study [64], although for a rather different parameter $\alpha = 0.36$. For the gap-corrected value $\alpha = 0.38$, we find a negative value $\Delta_{nK} = -0.4$ eV (Table 11.1), indicating concave $E(N)$ behavior, *i.e.*, overcorrection relative to the underlying DFA. Therefore, the corresponding acceptor level at 2.1 eV is most likely unrealistically deep. From the cancellation of the $E(N)$ non-linearity in different functional, as summarized in Table 11.1, we can conclude on theoretical grounds that shallow acceptor states that have been reported in ZnO [74–76] cannot originate from substitutional N_O impurities, and must have other causes. One recent suggestion is that the shallow levels are related to stacking faults, possibly decorated with additional defects or impurities [77].

11.5
The Balance Between Localization and Delocalization

In Ref. [78], we described two fundamentally different behaviors an electrically active defect (*i.e.*, a donor or an acceptor) can assume: (i) the primary defect-localized state (DLS), which results from the atomic orbital interaction between the defect atom and

its ligands, forms a resonance inside the continuum of host bands. In this case of a shallow defect, the carriers (electrons or holes) occupy a secondary perturbed host state (PHS) with a delocalized, band-like wavefunction and an energy close to the band edge. (ii) The DLS lies inside the band gap. This is the signature of a deep defect state, and the wavefunction is usually localized at the site of the defect and its ligands.

Even though Li is clearly a deep acceptor in ZnO on account of its large ionization energy and the localized nature of the bound hole [19], it is an interesting observation that the charged Li_{Zn}^{-} acceptor does not show a quasi-particle energy state inside the band gap, as shown in Figure 11.6a, and therefore shows the signature of the case (i) of a shallow state. In its equilibrium structure, the ionized Li acceptor exhibits no symmetry breaking, and all nearest neighbor are practically equal ($d_{Li-O} = 2.0$ Å) as expected from the approximate local T_d symmetry in the wurtzite lattice [79]. The large anisotropy in the NN-distances (*cf.* Figure 11.4a) occurs only after a hole is bound on one of the four initially equivalent O neighbors. One can, therefore, raise the "Chicken or egg" like question whether the hole localization causes the symmetry breaking of the atomic structure, or whether the symmetry breaking drives the hole localization. The answer to this question depends on whether the hole localizes on a single O-site even in the absence of the lattice distortion, or, in other words, whether there exists an energy barrier in the configuration coordinate diagram that causes

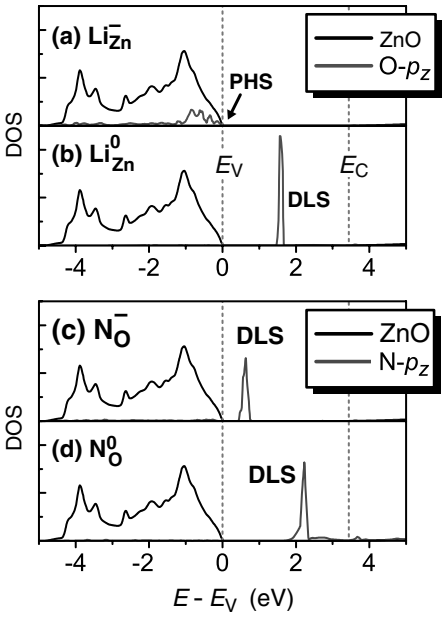

Figure 11.6 (online colour at: www.pss-b.com) Density of states (DOS) for the ionized and charge-neutral Li_{Zn} and N_O acceptor states in ZnO, calculated in DFA + V_{hs} (see Ref. [73]). The local DOS is projected on the O-p_z and N-p_z orbitals which host the bound hole in case of the charge-neutral acceptors (*cf.* Figures 11.1b and 11.5b, respectively).

a local minimum for the symmetric structure. Indeed, in the special situation that one defect, depending on its charge state, can assume both behaviors (i) and (ii) above, there exists generally an energy barrier between the two structural configurations. Such a barrier in the configuration coordinate diagram leads often to a range of experimentally observable metastability effects [78, 80, 81]. As seen in Figures 11.6a and b, the Li acceptor in ZnO indeed exhibits a change between shallow (i) and deep (ii) behavior being associated with a change of the charge state, which hints toward the presence of metastability effects.

Due to the energy of the Li-induced DLS below the VBM (Figure 11.6a), a free a hole can become bound at the Li acceptor in a effective-mass like (VBM-like) state without occupying the localized defect state. This shallow state of Li is, however only a transient state [82], because the energy can be lowered by the activated lattice relaxation and ensuing localization of the hole (Figure 11.1b) in a deep gap state (Figure 11.6b). Even though the transient shallow state is not suited to produce *p*-type conductivity, it could be observed for a short time after photo-excitation, thereby explaining the experimental observation of both a shallow and a deep state of the Li acceptor in photoluminescence [83, 84]. We recently [82] found a similar duality also for the metal-site acceptors in GaN, where Mg-doping has led to the observation of two distinct acceptor states in optical experiments [85] and of both effective-mass like and non-effective mass like hole wavefunctions in magnetic resonance experiments [86, 87]. We found that the ground state of the divalent acceptors Be, Mg, and Zn in GaN has always a localized hole wavefunction, akin to that of Li in ZnO (Figure 11.1b), which is indicative of a deep acceptor. However, Mg_{Ga} represents the unique case where the ionization energy of the deep state exceeds only slightly (by 0.03 eV) that of the ideal effective mass state, and is therefore still small enough for effective *p*-type doping. This explains the exceptional success of Mg-acceptor doping in GaN [88].

More generally, in regard of the balance between localization and delocalization, and the existence of an energy barrier, one can distinguish a total of four different cases, as illustrated in Figure 11.7. We now describe each case briefly with a specific example:

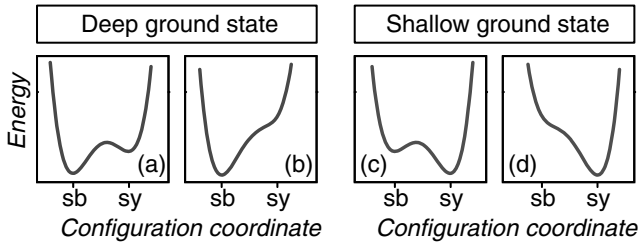

Figure 11.7 (online colour at: www.pss-b.com) Schematic configuration coordinate diagrams for acceptor states in semiconductors, illustrating the four different cases resulting from the energy ordering of the symmetry-broken (sb) and symmetric (sy) configurations, and from the existence or non-existence of an energy barrier.

i) *Deep ground state with barrier* (Figure 11.7a, *e.g.*, ZnO:Li). In the symmetric structure of the ionized Li_{Zn} acceptor, there is no defect induced quasi-particle state inside the band gap (Figure 11.6a). Thus, the neutral Li acceptor has a locally stable symmetric configuration with a delocalized effective-mass like wavefunction (PHS). Only after an activated symmetry breaking and large lattice relaxation, the localized O-p_z like hole state (*cf.* Figure 11.1b) occurs as a deep quasi-particle state (DLS) inside the band gap (Figure 11.6b). Examples include ZnO:Li_{Zn}, GaN:Mg_{Ga} [82], and ZnTe:V_{Zn} [20].

ii) *Deep ground state without barrier* (Figure 11.7b, *e.g.*, ZnO:N). The symmetric, ionized N_O acceptor (*cf.* Table 11.1) has its quasi-particle defect state already deep inside the band gap (Figure 11.6c). When forming the neutral acceptor state by removing an electron, the resulting hole immediately occupies the deep defect state (DLS), leading to the relaxation into the symmetry-broken configuration (*cf.* Table 11.1) without barrier. During relaxation, the DLS moves deeper into the gap (Figure 11.6c). Examples include ZnO:N_O [68] and ZnO:V_{Zn} [20].

iii) *Shallow ground state with barrier* (Figure 11.7c, *e.g.*, ZnTe:Li). So far, we have considered only acceptor states whose (charge neutral) ground states are symmetry broken and have a localized hole state. Of course, there exist also acceptors in semiconductors where the ground state is symmetric with a band like effective-mass wavefunction. Considering Li_{Zn} in ZnTe, we can utilize an initial lattice distortion to obtain a symmetry-broken state where the hole is located at only one of the four equivalent Te ligands, akin to the state shown in Figure 11.1b for ZnO. The parameter $\lambda_{hs} = 3.1$ eV for Te-p is then calculated analogous to the case of ZnO (Figure 11.4). However, we find that the T_d symmetric ground state with a delocalized effective-mass like hole wavefunction (PHS) lies 0.3 eV lower in energy than the symmetry-broken configuration. Thus, the generalized Koopmans formalism correctly predicts the well established effective-mass behavior of Li_{Zn} in ZnTe, and the calculated Li acceptor ionization energy of 0.08 eV reflects the shallow effective-mass acceptor level (experiment: 0.06 eV [89]).

iv) *Shallow ground state without barrier* (Figure 11.7d, *e.g.*, GaAs:Mg_{Ga}). For the Mg acceptor in GaAs, we find that the symmetry broken configuration cannot be stabilized even for large values of λ_{hs} for As-p (we can estimate $\lambda_{hs} = 2.7$ eV by evaluating the Koopmans condition for a constrained lattice distortion). Thus, the Mg_{Ga} acceptor in GaAs has only one energy minimum, *i.e.*, the T_d symmetric, shallow effective-mass state.

11.6 Conclusions

The physical condition of the piecewise linearity of the total energy $E(N)$ as a function of the fractional electron number plays an important role for the prediction of the structural configuration, the wave-function localization, and in particular, the

ionization energies of acceptors in wide-gap semiconductors. Based on DFT this condition may be achieved via on-site potentials or by mixing of non-local Fock exchange. When the bias of standard DFT toward symmetrical and delocalized solutions is overcome in such Koopmans corrected calculations, a symmetry broken solution often emerges as the ground state, usually leading to a deep non-conductive state (with the notable exception of GaN:Mg). The symmetry breaking of the defect wavefunction can either be the result of an initial breaking of the structural symmetry, or be purely electronically driven, corresponding to the existence or non-existence, respectively, of an energy barrier in the configuration coordinate diagram. In smaller-gap semiconductors with heavier anions the tendency toward hole localization is reduced, leading to shallow effective mass like states of substitutional acceptors.

Acknowledgements

This research was supported by the U.S. Department of Energy under Contract No. DE-AC36-08GO28308 and used high performance computing resources of the National Energy Research Scientific Computing Center.

References

1 Woodyard, J.R. (1944) US Patent No. 2,530,110 filed, June 2, 1944, awarded Nov. 14, 1950.
2 Pantelides, S.T. (ed) (1986) *Deep Centers in Semiconductors: A State of the Art Approach*, Gordon and Breach, Yverdon.
3 Schirmer, O.F. (2006) *J. Phys.: Condens. Matter*, **18**, R667.
4 Hohenberg, P. and Kohn, W. (1964) *Phys. Rev.*, **136**, B864.
5 Kohn, W. and Sham, L.J. (1965) *Phys. Rev.*, **140**, A1133.
6 von Barth, U. and Hedin, L. (1972) *J. Phys. C*, **5**, 1629.
7 Ceperley, D.M. and Alder, B.J. (1980) *Phys. Rev. Lett.*, **45**, 566.
8 Perdew, J.P. and Zunger, A. (1981) *Phys. Rev. B*, **23**, 5048.
9 Lee, C., Yang, W., and Parr, R.G. (1988) *Phys. Rev. B*, **37**, 785.
10 Perdew, J.P. and Wang, Y. (1992) *Phys. Rev. B*, **45**, 13244.
11 Perdew, J.P., Burke, K., and Ernzerhof, M. (1996) *Phys. Rev. Lett.*, **77**, 3865.
12 O'Brien, M.C.M. (1955) *Proc. R. Soc. Lond. A*, **231**, 404.
13 Schneider, J. and Schirmer, O.F. (1963) *Z. Naturf.*, **18a**, 20.
14 Vlasenko, L.S. and Watkins, G.D. (2005) *Phys. Rev. B*, **72**, 035203.
15 Wang, X.J., Vlasenko, L.S., Pearton, S.J., Chen, W.M., and Buyanova, I.A. (2009) *J. Phys. D, Appl. Phys.*, **42**, 175411.
16 Jeon, D.Y., Gislason, H.P., and Watkins, G.D. (1993) *Phys. Rev. B*, **48**, 7872.
17 Pacchioni, G., Frigoli, F., Ricci, D., and Weil, J.A. (2000) *Phys. Rev. B*, **63**, 054102.
18 Lægsgaard, J. and Stokbro, K. (2001) *Phys. Rev. Lett.*, **86**, 2834.
19 Lany, S. and Zunger, A. (2009) *Phys. Rev. B*, **80**, 085202.
20 Chan, J.A., Lany, S., and Zunger, A. (2009) *Phys. Rev. Lett.*, **103**, 016404.
21 Du, M.H. and Zhang, S.B. (2009) *Phys. Rev. B*, **80**, 115217.
22 Lichanot, A., Larrieu, C., Zicovich-Wilson, C., Roetti, C., Orlando, R., and Dovesi, R. (1998) *J. Phys. Chem. Solids*, **59**, 1119.
23 To, J., Sokol, A.A., French, S.A., Kaltsoyannis, N., and Catlow, C. R.A. (2005) *J. Chem. Phys.*, **122**, 144704.

24 Carvalho, A., Alkauskas, A., Pasquarello, A., Tagantsev, A.K., and Setter, N. (2009) *Phys. Rev. B*, **80**, 195205.
25 Gallino, F., Di Valentin, C., Pacchioni, G., Chiesa, M., and Giamello, E. (2010) *J. Mater. Chem.*, **20**, 689.
26 Clark, S.J., Robertson, J., Lany, S., and Zunger, A. (2010) *Phys. Rev. B*, **81**, 115311.
27 Nolan, M. and Watson, G.W. (2006) *J. Chem. Phys.*, **125**, 144701.
28 Elfimov, I.S., Rusydi, A., Csiszar, S.I., Hu, Z., Hsieh, H.H., Lin, H.-J., Chen, C.T., Liang, R., and Sawatzky, G.A. (2007) *Phys. Rev. Lett.*, **98**, 137202.
29 Morgan, B.J. and Watson, G.W. (2009) *Phys. Rev. B*, **80**, 233102.
30 Scanlon, D.O., Walsh, A., Morgan, B.J., Nolan, M., Fearon, J., and Watson, G.W. (2007) *J. Phys. Chem. C*, **111**, 7971.
31 d'Avezac, M., Calandra, M., and Mauri, F. (2005) *Phys. Rev. B*, **71**, 205210.
32 Droghetti, A., Pemmaraju, C.D., and Sanvito, S. (2008) *Phys. Rev. B*, **78**, 140404(R).
33 Kittel, C. and Mitchell, A.H. (1954) *Phys. Rev.*, **96**, 1488.
34 Luttinger, J.M. and Kohn, W. (1955) *Phys. Rev.*, **97**, 869.
35 Wardle, M.G., Goss, J.P., and Briddon, P.R. (2005) *Phys. Rev. B*, **71**, 155205.
36 Park, C.H., Zhang, S.B., and Wei, S.H. (2002) *Phys. Rev. B*, **66**, 073202.
37 Schirmer, O.F. and Zwingel, D. (1970) *Solid State Commun.*, **8**, 1559.
38 Meyer, B.K., Alves, H., Hofmann, D.M., Kriegseis, W., Forster, D., Bertram, F., Christen, J., Hoffmann, A., Straßburg, M., Dworzak, M., Haboeck, U., and Rodina, A.V. (2004) *Phys. Status Solidi B*, **241**, 231.
39 Becke, A.D. (1993) *J. Chem. Phys.*, **98**, 1372; (1993) *J. Chem. Phys.*, **98**, 5648.
40 Perdew, J.P., Ernzerhof, M., and Burke, K. (1996) *J. Chem. Phys.*, **105**, 9982.
41 Heyd, J., Scuseria, G.E., and Ernzerhof, M. (2003) *J. Chem. Phys.*, **118**, 8207; Krukau, A.V., Vydrov, O.A., Izmaylov, A.F., Scuseria, G.E. (2006) *J. Chem. Phys.*, **125**, 224106.
42 Perdew, J.P., Parr, R.G., Levy, M., and Balduz, J.L., Jr. (1982) *Phys. Rev. Lett.*, **49**, 1691.
43 Perdew, J.P., Ruzsinszky, A., Csonka, G.I., Vydrov, O.A., Scuseria, G.E., Staroverov, V.N., and Tao, J. (2007) *Phys. Rev. A*, **76**, 040501(R).
44 Mori-Sánchez, P., Cohen, A.J., and Yang, W. (2008) *Phys. Rev. Lett.*, **100**, 146401.
45 Slater, J.C., *Quantum Theory of Molecules and Solids*, Vol. 4 (1974) McGraw-Hill, New York.
46 Janak, J.F. (1978) *Phys. Rev. B*, **18**, 7165.
47 Perdew, J.P. and Levy, M. (1983) *Phys. Rev. Lett.*, **51**, 1884.
48 Sham, L.J. and Schlüter, M. (1983) *Phys. Rev. Lett.*, **51**, 1888.
49 Lany, S. and Zunger, A. (2008) *Phys. Rev. B*, **78**, 235104.
50 Koopmans, T.C. (1934) *Physica*, **1**, 104.
51 Zunger, A. and Freeman, A.J. (1977) *Phys. Rev. B*, **16**, 2901.
52 Anisimov, V.I., Solovyev, I.V., Korotin, M.A., Czyzyk, M.T., and Sawatzky, G.A. (1993) *Phys. Rev. B*, **48**, 16929.
53 Dudarev, S.L., Botton, G.A., Savrasov, S.Y., Humphreys, C.J., and Sutton, A.P. (1998) *Phys. Rev. B*, **57**, 1505.
54 Lany, S. and Zunger, A. (2009) *Modelling Simul. Mater. Sci. Eng.*, **17**, 084002.
55 Lany, S., Raebiger, H., and Zunger, A. (2008) *Phys. Rev. B*, **77**, 241201(R).
56 Lany, S. and Zunger, A. (2010) *Phys. Rev. B*, **81**, 113201.
57 Stoneham, A.M., Gavartin, J., Shluger, A.L., Kimmel, A.V., Muñoz Ramo, D., Rønnow, H.M., Aeppli, G., and Renner, C. (2007) *J. Phys.: Condens. Matter*, **19**, 255208.
58 Bylander, B.M. and Kleinman, L. (1990) *Phys. Rev. B*, **41**, 7868.
59 Asahi, R., Mannstadt, W., and Freeman, A.J. (1999) *Phys. Rev. B*, **59**, 7486.
60 Robertson, J., Xiong, K., and Clark, S.J. (2006) *Thin Solid Films*, **496**, 1.
61 Patterson, C.H. (2006) *Phys. Rev. B*, **74**, 144432.
62 Gali, A., Hornos, T., Son, N.T., Janzén, E., and Choyke, W.J. (2007) *Phys. Rev. B*, **75**, 045211.
63 Oba, F., Togo, A., Tanaka, I., Paier, J., and Kresse, G. (2008) *Phys. Rev. B*, **77**, 245202.
64 Lyons, J.L., Janotti, A., and Van de Walle, C.G. (2009) *Appl. Phys. Lett.*, **95**, 252105.

65 Islam, M.M., Bredow, T., and Gerson, A. (2007) *Phys. Rev. B*, **76**, 045217.

66 Stroppa, A. and Kresse, G. (2009) *Phys. Rev. B*, **79**, 201201(R).

67 Deák, P., Aradi, B., Frauenheim, T., Janzén, E., and Gali, A. (2010) *Phys. Rev. B*, **81**, 153203.

68 Lany, S. and Zunger, A. (2010) *Phys. Rev. B*, **81**, 205209.

69 McCluskey, M.D. and Jokela, S.J. (2009) *J. Appl. Phys.*, **106**, 071101.

70 Carlos, W.E., Glaser, E.R., and Look, D.C. (2001) *Phys. B*, **308–310**, 976.

71 Brant, A.T., Yang, S., Evans, S.M., Halliburton, L.E., and Giles, N.C. (2009) Mater. Res. Soc. Fall meeting, abstract H10.46

72 Due to the small DFA band gap, the N_O state hybridizes with the conduction band when $\lambda_{hs} > 3$ eV, which prevents the accurate calculation of $E(N+1)$. Therefore, we determined $\lambda_{hs} = 4.3$ eV by linear extrapolation of the difference $E(N+1) - E(N) - e_i$ between $1\text{ eV} \leq \lambda_{hs} \leq 3\text{ eV}$. Also, since a minimum threshold exists for λ_{hs} to produce the correct wave-function symmetry (see Figure 5), we determined the non-Koopmans energy Δ_{nK} for DFA (see Table 1) by back-extrapolation of the same linear function to $\lambda_{hs} = 0$.

73 For the underlying DFA we used the gradient corrected exchange correlation potential of Ref. [11] and an on-site Coulomb interaction [53] for Zn-d with $U = 6$ eV, see Ref. [49]. The conduction band edge was shifted to reflect the experimental band gap.

74 Zeuner, A., Alves, H., Hofmann, D.M., Meyer, B.K., Hoffmann, A., Haboeck, U., Strassburg, M., and Dworzak, M. (2002) *Phys. Status Solidi B*, **234**, R7.

75 Pan, M., Nause, J., Rengarajan, V., Rondon, R., Park, E.H., and Ferguson, I.T. (2007) *J. Electron. Mater.*, **36**, 457.

76 Liu, W., Gu, S.L., Ye, J.D., Zhu, S.M., Wu, Y.X., Shan, Z.P., Zhang, R., Zheng, Y.D., Choy, S.F., Lo, G.Q., and Sun, X.W. (2008) *J. Cryst. Growth*, **310**, 3448.

77 Schirra, M., Schneider, R., Reiser, A., Prinz, G.M., Feneberg, M., Biskupek, J., Kaiser, U., Krill, C.E., Thonke, K., and Sauer, R. (2008) *Phys. Rev. B*, **77**, 125215.

78 Lany, S. and Zunger, A. (2005) *Phys. Rev. B*, **72**, 035215.

79 The fact that the C3v point group symmetry of the wurtzite lattice sites is already lower than the Td symmetry plays practically no role for the present discussion. Analogous effects are observed also in the zincblende modification of ZnO [20].

80 Lany, S. and Zunger, A. (2004) *Phys. Rev. Lett.*, **93**, 156404.

81 Lany, S. and Zunger, A. (2006) *J. Appl. Phys.*, **100**, 113725.

82 Lany, S. and Zunger, A. (2010) *Appl. Phys. Lett.*, **96**, 142114.

83 Meyer, B.K., Volbers, N., Zeuner, A., Sann, J., Hofmann, A., and Haboeck, U. (2006) *Mater. Res. Soc. Symp. Proc.*, **891**, 491.

84 Meyer, B.K., Stehr, J., Hofstaetter, A., Volbers, N., Zeuner, A., and Sann, J. (2007) *Appl. Phys. A*, **88**, 119.

85 Monemar, B., Paskov, P.P., Pozina, G., Hemmingsson, C., Bergman, J.P., Kawashima, T., Amano, H., Akasaki, I., Paskova, T., Figge, S., Hommel, D., and Usui, A. (2009) *Phys. Rev. Lett.*, **102**, 235501.

86 Glaser, E.R., Carlos, W.E., Braga, G.C.B., Freitas, J.A., Jr., Moore, W.J., Shanabrook, B.V., Henry, R.L., Wickenden, A.E., Koleske, D.D., Obloh, H., Kozodoy, P., DenBaars, S.P., and Mishra, U.K. (2002) *Phys. Rev. B*, **65**, 085312.

87 Glaser, E.R., Murthy, M., Freitas, J.A., Jr., Storm, D.F., Zhou, L., and Smith, D.J. (2007) *Physica B*, **401-402**, 327.

88 Nakamura, S., Mukai, T., Senoh, M., and Iwasa, N. (1992) *Jpn. J. Appl. Phys.*, **31**, L139.

89 Magnea, N., Bensahel, D., Pautrat, J.L., and Pfister, J.C. (1979) *Phys. Status Solidi B*, **94**, 627.